SEISMIC VELOCITY STUDY OF THE RIM UPLIFT OF THE STEEN RIVER IMPACT CRATER. M. Niccoli, A.R. Hildebrand, and D.C. Lawton. Department of Geology and Geophysics, University of Calgary, Calgary AB Canada T2N 1N4; mniccoli@ucalgary.ca, ahildebr@ucalgary.ca., lawton@ucalgary.ca

Introduction. The buried ~25 km-diameter Steen River impact structure of Alberta is the remnant of the largest known crater in the Western Canadian Sedimentary Basin. The crater has no surface expression [1] and is defined by information derived from seismic data, well logs, and information from potential fields studies [2]. Several exploration wells drilled on the crater rim have encountered significant errors in depth prediction at the Slave Point level due to undetected high velocity areas creating apparent pull-ups, probably related to lateral variations in structure below the Cretaceous unconformity. Previous crater studies [3,4] have shown that an accurate velocity model is critical to characterize impact structures in depth, and can be derived with seismic techniques. Complementary refraction and reflection seismic studies have been completed to improve knowledge of the structural complexity at the rim of the Steen River crater.

Refraction experiment description. Autonomous Orion seismometers recorded a seismic reflection line shot approximately parallel to the crater's rim. Data were extracted with programs developed in Perl, and processed in Promax with a standard refraction flow. First breaks were picked and exported to Hampton-Russel's GLI3D, to create depth and velocity models using the General Linearized Inversion (GLI) method of [5]. Constraints from well logs aided the construction of the initial depth model to be ray traced. Based on density logs, a 3-layer density model has been proposed [6] as representative for the crater. In that model, Cretaceous shales form the top layer, with Devonian carbonates and shales below the Cretaceous unconformity, and then a lower section of Devonian carbonates and anhydrites overlying the Precambrian basement. Based on examination of the sonic logs and of the first break time curves, a 3-layer velocity model also seemed the most appropriate, with the top of layer 2 as the Cretaceous unconformity, and the top of layer 3 as the top of the Slave Point Formation. A 2D depth and velocity model was created; a 3D model was also created to compare to the 2D model. The first line modeled is located roughly along the rim uplift of the crater just outside the zone of slumping. In consequence, the line has varying azimuths. It also had faster formations at shallower depths on the outside of the rim versus the interior. This makes a 3D model necessary to explore the possible influence of out-of-plane refractions on the modeled velocities and depths. Having constrained the depths to tops of layer 2 and layer 3 using formation tops depths from vertical wells along the line, forces GLI3D to use lower velocities in the case of out of plane refractions, when modeling in 2D.

Discussion. The 2D model and a 2D section extracted from the 3D model are compared in Figure 1. The top displays in the figure show the modeled velocities. Layer 2 and layer 3 velocities have slightly lower values in the 3D model at both Orion 1 and Orion 2 locations. The two models yield similar velocities at the Orion 3 location, providing confidence in the velocities at this location. The bottom displays in Figure 1 show the post-stack Kirchhoff time migrated seismic line with superimposed GLI models, 2D in (a) and 3D in (b), respectively. To allow the superposition, both the 2D and 3D depth models have been converted to pseudo-time models. Inspection of these overlays offers useful insights. Both the 2D and 3D algorithms have accurately modeled the Cretaceous unconformity. As for the Slave Point, the 2D algorithm has failed to model the topography of the top of the formation even though constrained using the depths to the formation top from the wells available along the line. The 3D algorithm, on the other hand, has been successful in modeling the anticline in the Slave Point top below Orion 2. Below Orion 1, the 3D algorithm hasn't well modeled the anticline and has located the formation top at too great a depth. This, however, must be considered in light of the constant coefficients used to convert the depth model into a pseudo-time model. The 3D depth-velocity field was refined using GLI3D's tomographic algorithm, then interpolated in Matlab to create a regular grid and converted to time using an offset varying time to depth velocity conversion, and was finally superimposed on post-stack Kirchhoff time migration section. This final model is displayed in Figure 2 and better matches the folds in the rim uplift.

Reflection experiment description. A complementary study has been completed with determination of interval velocities on the concentric line and also a radial line intersecting it over the rim. Both lines were provided by Penn West Petroleum, Calgary, Alberta, Canada. Stacking velocity analysis on reflection CDP (common depth point) gathers can provide estimation of RMS velocities (root mean square, as defined in [7]), which can be used to calculate interval velocities using Dix equation [8]. If calculated over small increments, interval velocities approximate local instantaneous velocities and therefore are considered the most accurate representation of the real properties of the rocks in the subsurface. Because of the complex geology associated with the Steen River structure, Dip moveout (DMO) correction has been included in the processing flow to make the RMS velocities estimation dip independent. Data processing has been carried out at Geo-X Systems in Calgary. The processing flow is adapted from [7]. Geo-X's DMO correction operator is based on the Log Stretch Method of [9]. The velocity picking has been carried out with Geo-X's proprietary Variable Velocity Stacks module, which allows velocity analysis on CDP gathers, and real time stack response to the picked velocity. The simultaneous use of a Quality Control (QC) display with overlay of picked time/velocity pairs, interpolated interval velocity field, and final stack, allowed construction of a structure consistent interval velocity model. Picking was also constrained using velocity/time pairs from well velocity logs converted to two-way travel time. With this procedure, we have determined interval velocities for 15 intervals every 30 CDP (corresponding to a horizontal distance of 900 m) for both lines. The time-interval velocity field was interpolated in Matlab to create a regular grid and

superimposed on post-stack Kirchhoff time migration sections.

Discussion. Figure 3 displays the derived interval velocities for the concentric line. It is evident from comparing the interval velocities to the tomographically derived velocities as presented in Figure 2, that working with interval velocities has allowed greater velocity resolution and consistency with the known geology than refraction techniques, as expected. In terms of vertical resolution, Figure 3 shows that the formations just below the Cretaceous Unconformity, with interval velocities ranging from ~4500 to ~5500 m/s, overlay formations with interval velocities ranging from ~2800 to ~4500 m/s. The method has allowed distinction of the slower, shalier formations in the stratigraphic column from the faster, more carbonatic ones. Seismic refraction modeling could only produce an averaging of the velocities between the unconformity and the top of the Slave Point. This can be seen in Figure 2, where the velocity between the Cretaceous Unconformity and the top of the Slave Point Formation increases monotonically with depth.

In terms of horizontal resolution, Figure 3 demonstrates that dramatic changes occur in the thickness of the above described fast formations. We interpret this as thickening induced by compressive tectonics that formed the transient rim uplift during the Steen River impact. Additional evidence for this structural interpretation is the presence of steeply dipping fault planes on the radial line, which are shown in Figure 4, labeled as A, B, and C. These high angle fault planes have allowed overthrusting during the compressive stage, and likely have been reactivated during the extensional stage that followed, which is responsible for the block slumping within the crater's rim uplift (one indication of this reactivation is the reflector labeled in Figure 4 as D, which hints at extensional fault-bend folding). The structural thickening is not continuously observed along the concentric direction owing to the variable nature of impact-related compressional deformation. Because the principal stress and the mass transfer were outward radially from the center of the crater to the crater's rim, there must have been significant volume adjustments due to the increased circumference (leading to extensional tectonics in the concentric direction), so that the structural thickening only affected certain circumference sectors. This can be observed in Figure 3; south of Orion 1 we can see the traces of fault planes A, B, and C, labeled as A^1, B^1, and C^1, respectively. North of Orion 1 the faults pinch together, and just east of the line intersection, all geologic contacts seem to be stratigraphic. At the north end of the line another event, labeled as E, lays at an oblique angle representing a contact of faster units over slower ones. Between the line intersection and Orion 2 the fast formations are missing. This study adds constraints for the refraction modeling and reveals the structural complexity at the crater's rim.

References. [1] Robertson (1997) Oklahoma Geol. Surv. Circular 100, 385-390. [2] Hildebrand et al. (1998) Am. Ass. Pet. Geol. Annual Convention abs., CD format. [3] Dypvik et al. (1996) Geology 24, 779-882. [4] Anderson (1980) Can. Jou. Expl. Geoph. 16, 7-18. [5] Hampson and Russel (1984) Jou. Can. Soc. Epl. Geoph. 20, 40-54. [6] Spectra Exploration Geoscience (1996) Industry report. [7] Yilmaz (2001) Seismic Data analysis, Society of Exploration Geophysics, 2 vol. [8] Dix (1955) Geophysics 20, 68-86. [9] Liner (1990) Geophysics 55, 595-607.

Aknowledgments. COURSE Program of Alberta Government, Penn West Petroleum, Geo-X Systems.

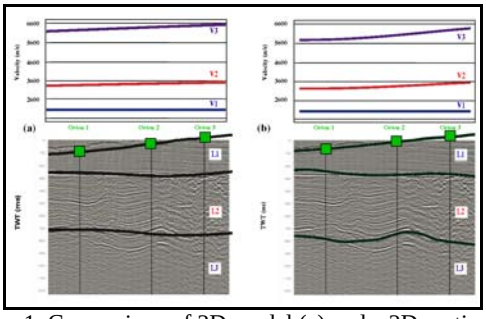

Figure 1. Comparison of 2D model (a) and a 2D section from a 3D model (b) for the concentric line.

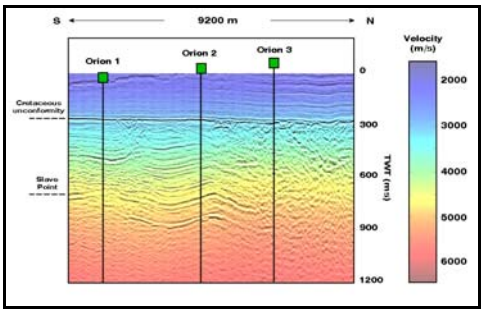

Figure 2. Overlay of a 2D section from the 3D tomographic model for the concentric line on post-stack time migration.

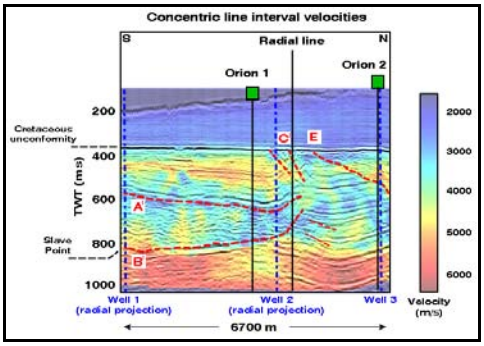

Figure 3. Overlay of concentric line interval velocities on post-stack time migration.

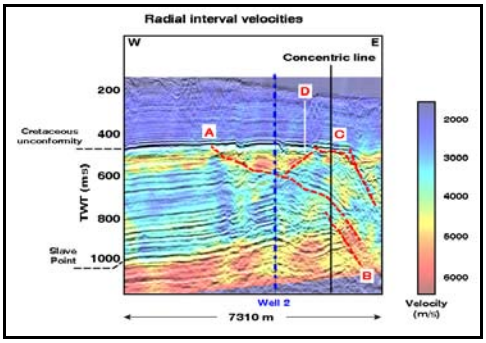

Figure 4. Overlay of radial line interval velocities on post-stack time migration.